RPE Radiation Physics & Engineering
An International Peer-Reviewed Journal
Published by K.N. Toosi University of Technology
http://rpe.kntu.ac.ir
Research Article

Radiation Physics and Engineering 2020; 1(3):11–16
https://doi.org/10.22034/RPE.2020.89327

Optimization of beamline diameter in spot scanning proton therapy for minimization of secondary particles using finite element method

Amir Veiskarami[a], Mahdi Sadeghi[b], Dariush Sardari[a], Shahryar Malekie[c,*]

[a] *Department of Medical Radiation Engineering, Science and Research Branch, Islamic Azad University, Tehran, Iran*
[b] *Iran University of Medical Sciences, Medical Physics Department, Tehran, Iran*
[c] *Radiation Application Research School, Nuclear Science & Technology Research Institute, PO Box 31485-498, Karaj, Iran*

HIGHLIGHTS

- Spot scanning proton therapy was simulated via the finite element method.
- The optimum diameter of proton beamline was determined to minimize the production of secondary particles.
- The forward particles exhibited greater velocities than those of rear particles.

ABSTRACT

Collision of protons with background gas and beamline wall in proton therapy causes the creation of secondary particles, *e.g.* neutrons, which results in more difficulties in curing the tumors. In the present simulation-based study, the optimum diameter of proton beamline was determined to minimize the production of secondary particles in the presence of electric field with the magnitude of 50 kV/m, perpendicular equal magnetic fields of 0.7 T, and background gas of argon under Bounce boundary conditions via finite element method. The results showed that the optimum diameter of the beamline for minimization of the secondary particles in the spot scanning proton therapy in the aforementioned conditions was 7 mm. Also, the values of drift velocities of protons were plotted in different time steps of 10 ns to 50 ns for the optimized size of the beamline. Due to few interactions of forwarding particles with background gas, the results showed that the forwarding particles in the propagation direction have greater velocities than those of rear particles. The results can be used in spot scanning proton therapy for curing the localized cancers.

KEYWORDS
Spot scanning proton therapy
Beamline diameter
Secondary particles
Finite element method

HISTORY
Received: 18 April 2018
Revised: 21 August 2018
Accepted: 23 October 2018
Published: July 2020

1 Introduction

Spot scanning proton therapy is particularly appropriate to become the favorite radiation modality for curing a wide variety of cancers (McDonald and Fitzek, 2010; Hyer et al., 2014; Poenisch et al., 2016; Schneider et al., 2002; Lomax et al., 2004; Smith et al., 2016). Owing to the fact that proton therapy is able to diminish the radiation absorbed in the volume of nontarget tissue, it is particularly promising for pediatric patients (McDonald and Fitzek, 2010). By decreasing the volume of irradiated tissue, proton therapy is believed to decrease both the risk of secondary malignancies and the extent of late normal tissue effects (McDonald and Fitzek, 2010). As proton therapy continues to evolve, wider implementation of active beam scanning and other technology promises to fully realize the promise of reduced dose to nontarget tissues, both directly absorbed dose from the incident beam and avoidable elements of scattered radiation (McDonald and Fitzek, 2010). The main advantage of proton therapy is the prevention of unnecessary doses in other organs adjacent to the cancerous tumor (Newhauser and Zhang, 2015). Considering the advantages of the Bragg peak, proton radiation delivers an insignificant dose to the normal tissues located after the peak position (McDonald and Fitzek, 2010; Ho et al., 2017; Søbstad, 2017; Yao et al., 2016; Ricardi et al., 2017; Chang et al., 2016). Proton therapy exhibits a wide range of potential applications namely: pediatric tumors (medulloblastoma, Rhabdomyosarcoma, ependymomas, gliomas, and craniopharyngiomas), central nervous system tumors (Glioblastoma).

Treatment of cancer cells using a scanning proton beam

*Corresponding author: smaleki@aeoi.org.ir

has been assessed to deliver conspicuously less dose due to the scattered radiation compared with that of photon radiation (Hall, 2006). Especially, however, most proton treatments are still delivered with passive beam modulation, which results in a more production of secondary neutrons, known as a source of scattered radiation with a high relative biological effectiveness (RBE) that might abolish some of the conspicuous dosimetric benefits of protons. Although it has been documented that passive proton scattering results in prominently high scatter neutron dose (Hall, 2006), others have demonstrated that with suitable beam collimation that reflects actual clinical use, the scattered neutron dose is in fact much lower (Jiang et al., 2005; Gottschalk, 2006).

In designing a treatment planning system for proton therapy using spot scanning method, van de Water *et al.* (van de Water et al., 2012) found that there is some scope for optimizing the number of spots delivered per field. Field-specific dosimetry shows that these treatments can be delivered accurately and precisely to ±1 mm (1 SD) orthogonal to the field direction and to within 1.5 mm in the depth of penetration (van de Water et al., 2012). The geometry of treatment planning system therefore plays an important role in the proton therapy. Several researchers have investigated the performance of spot scanning proton therapy in the world (McDonald and Fitzek, 2010; van de Water et al., 2012; Grevillot et al., 2011; Timmermann et al., 2007; Weber et al., 2005; Owen et al., 2014; Elnahal et al., 2013; Jansen et al., 2000; Lin et al., 2000; Lomax et al., 1999).

The Lorentz force applies on proton beam with the electric charge of q and velocity of v in the presence of electric field E and magnetic field B. By moving in the background gas, the protons loose their energy through Coulomb scattering. Moreover, elastic and non-elastic collisions with target nuclides cause to producing secondary particles such as neutrons, photons, and secondary protons. Because of the span of energies for protons in proton therapy (70-250 MeV), the most probable secondary particles are neutrons which can damage normal tissue due to their high radiation weighting factor. In order to decrease the dose due to the secondary neutrons in dosimetry studies, the beamline wall diameter is simulated optimally to prevent the production of secondary neutrons via interaction of protons with the beamline wall.

A cyclotron consists of dipole magnets has been designed to produce a region of a uniform magnetic field (Schlegel et al., 2008). The size of the magnets and the strength of the magnetic fields limit the energy of particle emitted from a cyclotron (Schlegel et al., 2008). The maximum proton beam energy relates to the maximum depth in tissue (Schlegel et al., 2008). In order to be able to deliver the protons to the tissue, a beamline is needed. In fact, particle accelerators apply electric fields to speed up and increase the energy of a beam of particles, which are steered and focused by magnetic fields.

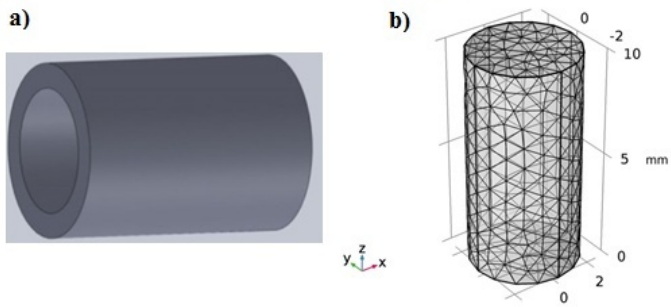

Figure 1: a) Schematic design of a proton beamline, b) Mesh processing for a proton beamline.

In proton therapy, the secondary neutrons are produced via two ways; They can be produced before arriving to the patient through collisions with the wall of beamline. This effect can be avoided by a suitable shielding. Furthermore, these particles can be produced in the patient's body via the collision with tissue. In this case, it is not possible to control them via mechanical instruments. The materials and geometry of the beamline are two essential factors in the production of secondary neutrons in the body.

Jia *et al.* (Jia et al., 2014) have reported that two most important secondary particles, *i.e.* neutrons and photons, are produced in the proton therapy in the range of 40-140 MeV. All "non-primary" particles are produced either by interactions of the primary protons or by the interactions of the secondary particles. Regarding the neutron and photon productions per primary protons, they reported that neutron and photon productions for E_p= 40 MeV ranges between 0.27% and 1.60%, respectively. For E_p= 140 MeV, these values change to 10.14% and 9.10%. They found that by increasing the beam energy, the production of secondary particles, especially neutrons, increases (Jia et al., 2014).

In the present theoretical work, the optimum diameter of proton beamline in order to minimize the production of secondary particles in the proton therapy was evaluated using the finite element method.

2 Simulation Methodology

Finite element method (FEM) is a numerical procedure to obtain solutions for boundary-value problems of mathematical physics (Reddy, 2005). In FEM, the system is divided into small subdomains, or elements, which are connected to each other by nodes (Malekie and Ziaie, 2017). Since finding the exact solution of time-dependent Newton equation for a complex system like beamline is a challenging issue, FEM can capture more details in predicting the interaction of protons with background gas and wall of beamline during the proton therapy. In this work, finite element method has been used for simulation of motion of protons in the beamline. Figure 1 shows a schematic view of a beamline and its mesh processing.

Argon was considered as background gas with the density of 2.956×10^{21} 1/m^3. In order to accelerate the pro-

tons in the beamline, electric field of $E_z = 50$ kV/m and magnetic fields of $B_x = B_y = 0.7$ T were considered. The charged particle tracing length in the beamline was considered as 10 mm. When a group of protons are accelerated in the neutral background gas, the Maxwellian velocity distribution can be considered as (COMSOL, 2013)

$$f(v_i) = \sqrt{\frac{m_p}{2\pi k_B T_0}} \exp(\frac{m_p v_i^2}{2k_B T_0}) \quad (1)$$

where $f(v_i)$ is the distribution function of Maxwellian velocity, v_i is the velocity, T_0 is gas temperature, k_B is Boltzmann constant, and m_p is mass of proton. Therefore, the elastic collision frequency of the protons with background gas can be calculated by (COMSOL, 2013)

$$\nu = \mathrm{N}_d\, \sigma |\nu_p - \nu_g| \quad (2)$$

where σ is the collision cross-section, N_d is the number of background gas, ν is collision frequency, ν_p is velocity of protons and ν_g is the velocity of the background gas. The collision cross-section is a function of kinetic energy of the particles. Hence, the probability of the collision, p, is calculated as a function of collision frequency and time step Δt as (COMSOL, 2013)

$$p = 1 - \exp(-\nu \Delta t) \quad (3)$$

As mentioned, although protons are affected by elastic collisions, a uniform electric field is applied on particles in the z-axis direction. It is possible to consider two boundary conditions for the beamline wall: Freeze and Bounce. In the Freeze boundary conditions, the collision of particles with the beamline wall is considered such that particles adhere to the beamline wall after a collision. In this case, the velocity of the particles at the moment of collision with the wall is zero and thus, in all time steps after the collision, the particle velocity is considered zero. For Bounce boundary conditions, the momentum of beamline particles in the collisions will be conservative (COMSOL, 2013)

$$\nu = \nu_c - 2(\mathrm{n}.\nu_c)\mathrm{n} \quad (4)$$

where ν_c and n are the velocity of the particles after the collision with wall and normal vector to the wall, respectively. In this simulation, since Bounce boundary condition is near to the reality, this method was chosen as wall boundary conditions in the collisions of protons with beamline wall. In fact, by solving Newton's equation for specified boundary conditions using $F = \frac{\mathrm{d}(m_p v)}{\mathrm{d}t}$ for protons with mass m_p, it is possible to obtain velocity of the particles that experience electric and magnetic fields of E and B, respectively for the Lorentz force. And also collision probability of the charged particles with the beamline wall is obtained from Eqs. (1) to (4). In this research, a commercial finite element solver (COMSOL Multiphysics) installed on a personal computer with 32 GB RAM and 3.4 GHz processor was used to numerically predict the charge particle tracing (COMSOL, 1994).

3 Results and Discussion

Figure 2 shows the collisions of particles with beamline wall in the $X - Y$ plane for different beamline diameter in the range of 2-4 mm in the time intervals of (equals to time-related to one pulse of the proton) plotted using the COMSOL Multiphysics Software version 5.3 a. It can be deduced that there is a minimum value of collisions between particles and the wall for the beamline radius of 3.5 mm. Considering the articles published so far, this amount is in accordance with some active beamline facilities to have 7 mm of FWHM at the skin surface (Jia et al., 2014; Kraft, 2000; Pedroni et al., 1995; Haberer et al., 1993). In this case, in the time related to one pulse, there is not enough time for particles to reach the beamline wall, the probability of producing the secondary particles therefore decreases.

Kinetic energy and the total number of incident particles of the beamline after 10 ns were calculated as 1.43×10^{-18} J and 2.7×10^4 J, respectively. These values seem to be small in comparison with real conditions in proton therapy, in which energy of protons reaches to 70-250 MeV. As can be seen from Figs. 3 and 4, the argon gas targets with 10 mm thicknesses cannot lead to a strong scattering of secondary particles. Since a large number of collisions happens during the time, so in this simulation we considered only small time intervals in the range of 10-50 ns. However, it should be mentioned that the kinetic energy of incident particles increases with time and because of limitations due to the computer processing, we considered such values to investigate the physical phenomena related to these collisions in small time intervals.

Figure 5 shows the values of drift velocities of protons plotted in different time steps, from 10 ns to 50 ns, for beamline wall of 3.5 mm radius. From this figure, it is evident that the forward particles in z-axis direction have a greater velocity than those of rear particles. In fact, the rear particles are affected by more interactions between protons that causes dissipation of kinetic energy of the particles and the velocity subsequently, while forward particles only interact with background gas, resulting in larger final velocity. In the simulation process, during solving Newton's equation for specified boundary conditions, the relative tolerance was kept at 0.00001, so it can be deduced that error calculation in this work is less than 0.001% regarding the mesh processing in the finite element method. To clarify this issue, the relative tolerance is related to the convergence criteria. Therefore, if the relative tolerance is reduced, the solution accuracy will be increased. However, there is a need to spend more time due to the fact that more number of iterations will be implemented. In other words, in finite element method, relative tolerance is pertinent to the fluctuation of the solution due to mesh processing and physics of the problem. Due to the three dimensional models solved numerically by finite element method, the selection of the appropriate mesh size (coarse, normal, fine, etc.) plays an important role in determination of the results.

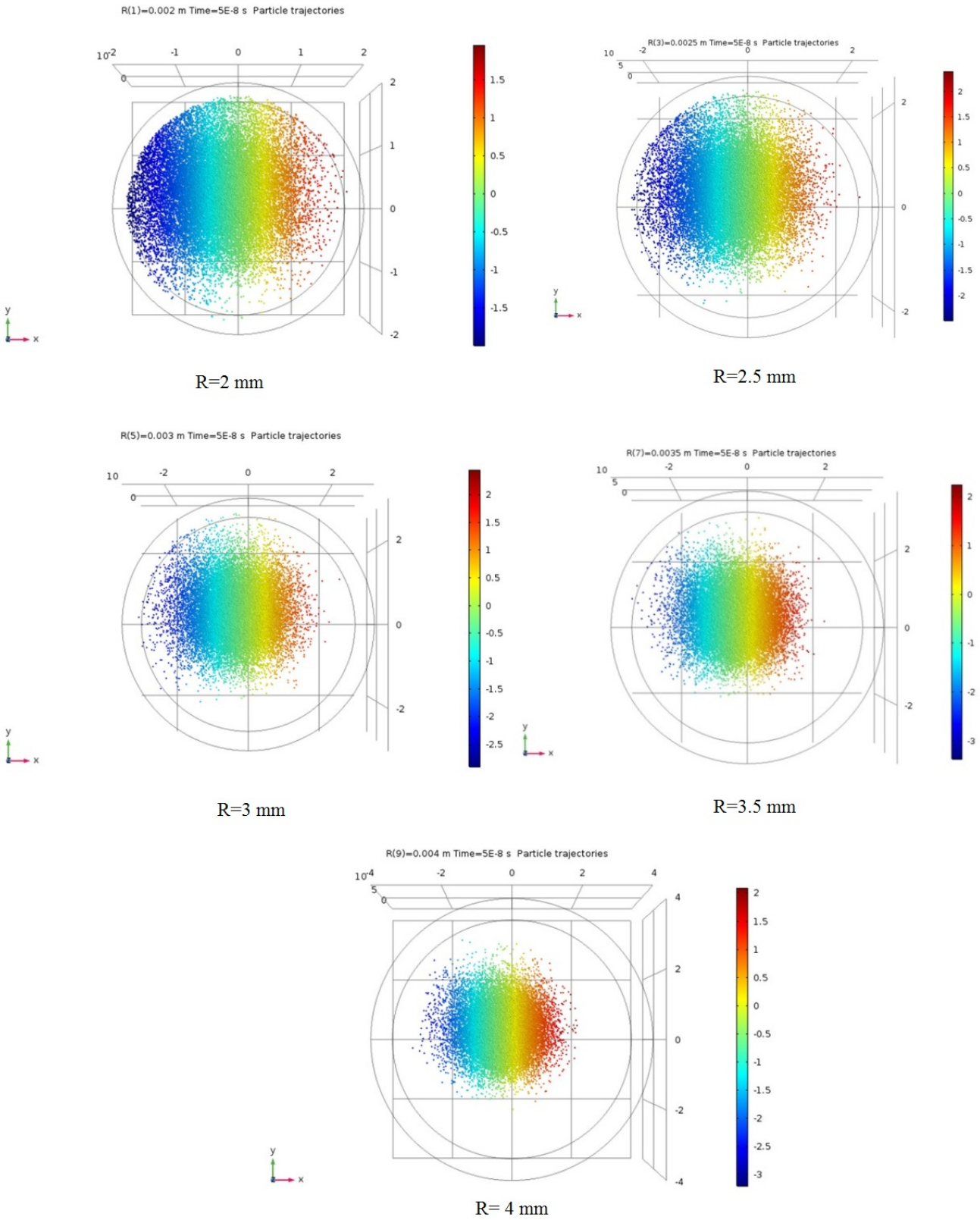

Figure 2: Collision of protons with the beamline wall of different radii. The colored data indicate the particle scattering radius, blue and red indicate the minimum and maximum diameter from -3 to 2 mm, respectively.

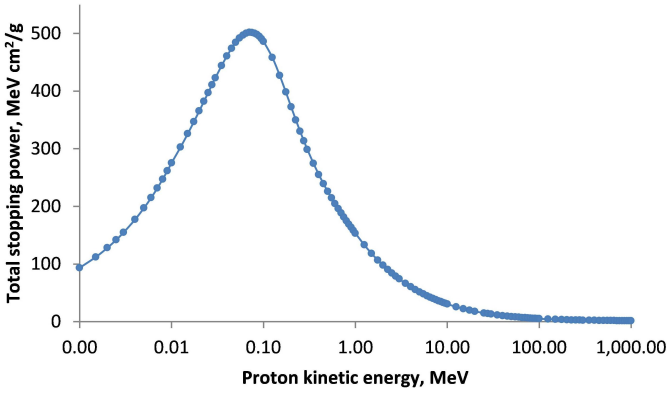

Figure 3: Total stopping power of protons in the argon gas for various energies (Deasy, 1994).

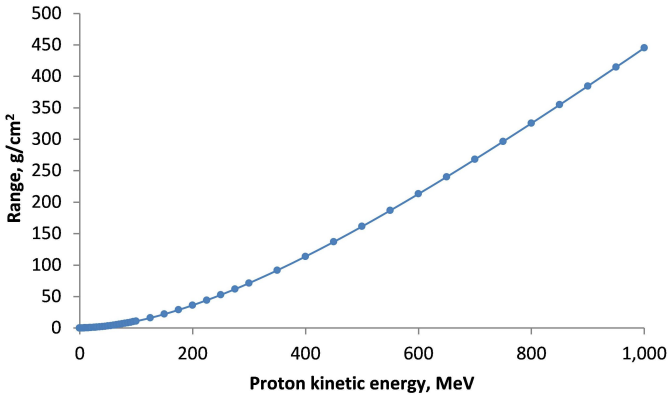

Figure 4: Range of protons in the argon gas for various energies (Deasy, 1994).

4 Conclusion

Evaluation of the geometry of beamline for achieving an optimum size for reducing the secondary particles is an important issue in the proton therapy. In this simulation study, the optimum diameter of proton beamline was estimated in the presence of the electric field of E_z =50 kV/m and magnetic fields of $B_x = B_y = 0.7$ T using finite element method. Regarding the Maxwellian velocity distribution of protons in the presence of argon as background gas, and Bounce boundary conditions for the interaction of protons with beamline wall as well, the results showed that the optimum diameter of the beamline for minimization of the secondary particles was 7 mm. This amount was in accordance with the literature. Finally, the values of drift velocities of protons were plotted in different time steps from 10 ns to 50 ns for the simulated optimized size of the beamline. The results showed that the forwarding particles in the propagation direction have a greater velocity than those of rear particles, which can be interpreted due to the fewer interactions of forwarding particles with background gas. The optimum beamline geometry helps the treatment planning to exhibit the lower amount of undesired dose to healthy organs. These useful calculations can capture more details in spot scanning proton therapy for curing the localized cancers.

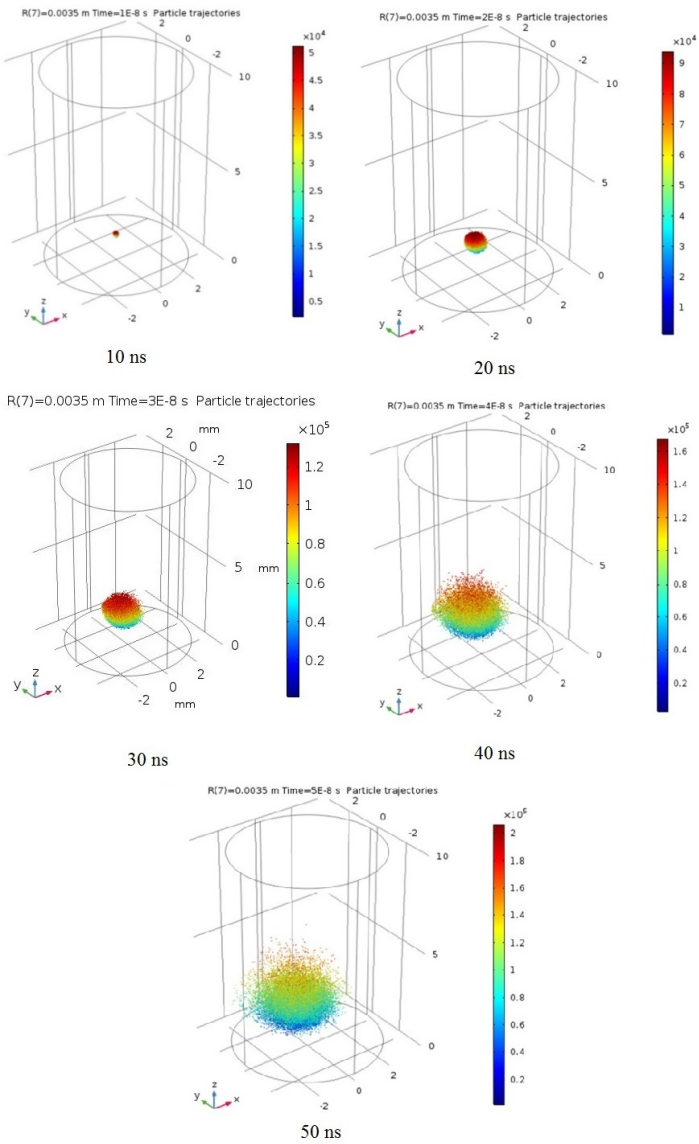

Figure 5: The drift velocity of protons in different time steps from 10 to 50 ns for beamline wall of 3.5 mm radius (the unit of drift velocity is m/s) using the COMSOL Multiphysics Software version 5.3 a.

References

Chang, J. Y., Jabbour, S. K., De Ruysscher, D., et al. (2016). Consensus statement on proton therapy in early-stage and locally advanced non–small cell lung cancer. *International Journal of Radiation Oncology* Biology* Physics*, 95(1):505–516.

COMSOL (1994). Guide, comsol multiphysics users. *Inc.-2006.-708 p.*

COMSOL (2013). Comsol multiphysics user guide (version 4.3 a). *COMSOL, AB*, pages 39–40.

Deasy, J. (1994). ICRU Report 49, stopping powers and ranges for protons and alpha particles. *Medical Physics*, 21(5):709–710.

Elnahal, S. M., Kerstiens, J., Helsper, R. S., et al. (2013). Proton beam therapy and accountable care: the challenges

ahead. *International Journal of Radiation Oncology* Biology* Physics*, 85(4):e165–e172.

Gottschalk, B. (2006). Neutron dose in scattered and scanned proton beams: In regard to Eric J. Hall (Int J Radiat Oncol Biol Phys 2006; 65: 1–7). *International Journal of Radiation Oncology* Biology* Physics*, 66(5):1594.

Grevillot, L., Bertrand, D., Dessy, F., et al. (2011). A Monte Carlo pencil beam scanning model for proton treatment plan simulation using GATE/GEANT4. *Physics in Medicine and Biology*, 56(16):5203.

Haberer, T., Becher, W., Schardt, D., et al. (1993). Magnetic scanning system for heavy ion therapy. *Nuclear Instruments and Methods in Physics Research Section A: Accelerators, Spectrometers, Detectors and Associated Equipment*, 330(1-2):296–305.

Hall, E. J. (2006). Intensity-modulated radiation therapy, protons, and the risk of second cancers. *International Journal of Radiation Oncology* Biology* Physics*, 65(1):1–7.

Ho, E. S., Barrett, S. A., and Mullaney, L. M. (2017). A review of dosimetric and toxicity modeling of proton versus photon craniospinal irradiation for pediatrics medulloblastoma. *Acta Oncologica*, 56(8):1031–1042.

Hyer, D. E., Hill, P. M., Wang, D., et al. (2014). Effects of spot size and spot spacing on lateral penumbra reduction when using a dynamic collimation system for spot scanning proton therapy. *Physics in Medicine and Biology*, 59(22):N187.

Jansen, E. P., Dewit, L. G., van Herk, M., et al. (2000). Target volumes in radiotherapy for high-grade malignant glioma of the brain. *Radiotherapy and Oncology*, 56(2):151–156.

Jia, S. B., Hadizadeh, M. H., Mowlavi, A. A., et al. (2014). Evaluation of energy deposition and secondary particle production in proton therapy of brain using a slab head phantom. *Reports of Practical Oncology and Radiotherapy*, 19(6):376–384.

Jiang, H., Wang, B., Xu, X. G., et al. (2005). Simulation of organ-specific patient effective dose due to secondary neutrons in proton radiation treatment. *Physics in Medicine and Biology*, 50(18):4337.

Kraft, G. (2000). Tumor therapy with heavy charged particles. *Progress in Particle and Nuclear Physics*, 45:S473–S544.

Lin, R., Hug, E. B., Schaefer, R. A., et al. (2000). Conformal proton radiation therapy of the posterior fossa: a study comparing protons with three-dimensional planned photons in limiting dose to auditory structures. *International Journal of Radiation Oncology* Biology* Physics*, 48(4):1219–1226.

Lomax, A. J., Böhringer, T., Bolsi, A., et al. (2004). Treatment planning and verification of proton therapy using spot scanning: Initial experiences. *Medical Physics*, 31(11):3150–3157.

Lomax, A. J., Bortfeld, T., Goitein, G., et al. (1999). A treatment planning inter-comparison of proton and intensity modulated photon radiotherapy. *Radiotherapy and Oncology*, 51(3):257–271.

Malekie, S. and Ziaie, F. (2017). A two-dimensional simulation to predict the electrical behavior of carbon nanotube/polymer composites. *Journal of Polymer Engineering*, 37(2):205–210.

McDonald, M. W. and Fitzek, M. M. (2010). Proton therapy. *Current problems in cancer*, 34(4):257.

Newhauser, W. D. and Zhang, R. (2015). The physics of proton therapy. *Physics in Medicine and Biology*, 60(8):R155.

Owen, H., Holder, D., Alonso, J., et al. (2014). Technologies for delivery of proton and ion beams for radiotherapy. *International Journal of Modern Physics A*, 29(14):1441002.

Pedroni, E., Bacher, R., Blattmann, H., et al. (1995). The 200-MeV proton therapy project at the Paul Scherrer Institute: Conceptual design and practical realization. *Medical Physics*, 22(1):37–53.

Poenisch, F., Gillin, M., Sahoo, N., et al. (2016). SU-F-T-165: Daily QA analysis for spot scanning beamline. *Medical Physics*, 43(6Part15):3499–3500.

Reddy, J. N. (2005). *An introduction to the finite element method. 3rd Edition*, volume 2. McGraw-Hill New York.

Ricardi, U., Dabaja, B., and Hodgson, D. (2017). Proton therapy in mediastinal Hodgkin lymphoma: moving from dosimetric prediction to clinical evidence.

Schlegel, W., Bortfeld, T., Grosu, A.-L., et al. (2008). New Technologies in Radiation Oncology. *Journal of Nuclear Medicine*, 49(4):683–684.

Schneider, U., Agosteo, S., Pedroni, E., et al. (2002). Secondary neutron dose during proton therapy using spot scanning. *International Journal of Radiation Oncology* Biology* Physics*, 53(1):244–251.

Smith, B., Gelover, E., Moignier, A., et al. (2016). A treatment plan comparison between dynamic collimation and a fixed aperture during spot scanning proton therapy for brain treatment. *Medical Physics*, 43(8Part1):4693–4699.

Søbstad, J. M. (2017). Monte Carlo based comparison of constant vs. variable RBE for proton therapy patients. Master's thesis, The University of Bergen.

Timmermann, B., Schuck, A., Niggli, F., et al. (2007). Spot-scanning proton therapy for malignant soft tissue tumors in childhood: First experiences at the Paul Scherrer Institute. *International Journal of Radiation Oncology* Biology* Physics*, 67(2):497–504.

van de Water, T. A., Lomax, A. J., Bijl, H. P., et al. (2012). Using a reduced spot size for intensity-modulated proton therapy potentially improves salivary gland-sparing in oropharyngeal cancer. *International Journal of Radiation Oncology* Biology* Physics*, 82(2):e313–e319.

Weber, D. C., Rutz, H. P., Pedroni, E. S., et al. (2005). Results of spot-scanning proton radiation therapy for chordoma and chondrosarcoma of the skull base: the Paul Scherrer Institut experience. *International Journal of Radiation Oncology* Biology* Physics*, 63(2):401–409.

Yao, W., Merchant, T. E., and Farr, J. B. (2016). A correction scheme for a simplified analytical random walk model algorithm of proton dose calculation in distal Bragg peak regions. *Physics in Medicine and Biology*, 61(20):7397.